*Original Article*

# Plasma-activated medium exerts tumor-specific inhibitory effect on hepatocellular carcinoma via disruption of the salvage pathway

**Yu Bai,[1] Chenwei Dai,[1] Nini Chen,[2] Xiuhong Zhou,[1] Hua Li,[3] Qinghua Xu,[4,*] and Yong Xu[1,*]**

[1]Anhui Academy of Medical Sciences, Anhui Medical College, Gongwan Road 15, Hefei City, Anhui Province, China
[2]School of Life Science, Anhui Agricultural University, Changjiang 130, Hefei City, Anhui Province, China
[3]School of Basic Medicine, Anhui Medical College, Furong Road 632, Hefei City, Anhui Province, China
[4]Anhui Provincial Center for Disease Control and Prevention, Fanhua Road 12560, Hefei City, Anhui Province, China

(Received 26 November, 2023; Accepted 10 January, 2024; Released online in J-STAGE as advance publication 26 January, 2024)

**Hepatocellular carcinoma has high fatality and poor prognosis. For curing hepatocellular carcinoma, the demand for effective therapeutic reagents with low toxicity is urgent. Herein, we investigated plasma-activated medium, an emerging reagent obtained via irradiation of cell-free medium with cold atmospheric plasma. Plasma-activated medium exerts inhibitory effect on many types of tumor cells with little toxicity to non-cancerous cells. In present study, we verified the tumor-specific inhibition of plasma-activated medium on hepatocellular carcinoma cell lines. Under the effect of plasma-activated medium, oxidative stress, mitochondrial dysfunction, and loss of intracellular $NAD^+$ and ATP were detected inside cells, suggesting an energy depletion. Through investigating the salvage pathway which synthesizes $NAD^+$ and maintains the respiratory chain in hepatocellular carcinoma, we found that the energy failure was resulted by the blockage of the salvage pathway. Moreover, nicotinamide phosphoribosyltransferase, the rate-limiting enzyme in the salvage pathway, was determined as an important target to be inactivated by the effect of plasma-activated medium. Additionally, the blockage of the salvage pathway activates AMPK$\alpha$ and suppresses mTOR pathway, which reinforces the cell growth inhibition. Overall, our findings demonstrated that the disruption of functions of nicotinamide phosphoribosyltransferase and the salvage pathway contribute to the tumor-specific cytotoxicity of plasma-activated medium.**

***Key Words*:** **plasma-activated medium, hepatocellular carcinoma, salvage pathway, NAMPT**

Hepatocellular carcinoma (HCC) is one of the most common malignant tumors worldwide and the second leading cause of cancer-related death.[1] HCC, once detected, is more likely to be advanced, owing to its rapid proliferation, high malignancy and great propensity to metastasize.[2] At the late stage of HCC, patients suffer from limited therapeutic means and very poor prognosis. Nowadays, the available options for treating HCC includes surgery, chemotherapy, radiotherapy, but in most cases, they present unsatisfactory curative effect and incur serious damage to normal liver function.[3] Thus, there is an increasing demand for the development of more effective and targeted and less harmful therapy against HCC.[4,5]

With growing knowledge of tumor physiology, the distinctive energy metabolism of most solid tumors including HCC emerges as a target of a great interest for development of new therapeutic strategies.[6] The energy metabolism of solid tumors including HCC is characterized by taking advantage of glycolysis without oxygen than oxidative phosphorylation pathway, namely Warburg effect, which substantially adapts HCC to its anoxic microenvironment.[7–9] In glycolysis pathway, nicotinamide adenine dinucleotide ($NAD^+$) is the only electron/proton ($H^•$) carrier, and functions as the coenzyme of glyceraldehyde 3-phosphate dehydrogenase to form NADH to ensure both glycolysis and respiratory chain proceeding normally. Therefore, HCC has a higher demand for $NAD^+$ than normal cells owing to its serious dependency upon glycolytic energy.[10] So far, three $NAD^+$ biosynthesis pathways have been discovered in mammalian cells, out of which only the salvage pathway exists completely in HCC cells and takes the responsibility of the provision of $NAD^+$.[8,10,11] The salvage pathway consists of two sequential key steps, where nicotinamide (NAM) is converted to nicotinamide mononucleotide (NMN) under the catalysis of nicotinamide phosphoribosyl transferase (NAMPT), and nicotinamide mononucleotide adenylyltransferase (NMNAT) catalyzes the condensation between NMN and ATP to generate $NAD^+$.[12] In this pathway, NAMPT is a rate-limiting enzyme, whose expression level and activity in HCC are significantly higher than that in normal cells, hence it has been becoming one of the most promising targets for HCC treatment.[13–16]

In previous studies on HCC and several other types of tumors, the down-regulation of NAMPT by either expression interference or inhibitory agents, could fundamentally interrupt the generation of intracellular $NAD^+$ and result in a dysfunction of glycolysis and a depletion of ATP.[17] Such a failure in energy metabolism halts a range of essential physiological events to cause cell death,[18,19] and up-regulation of AMP-activated protein kinase (AMPK) has been unraveled as one of the most outstanding downstream events.[20] AMPK is a major signaling enzyme for maintaining cellular energy homeostasis and coordinating multiple metabolic pathways.[21] AMPK is sensitive to cellular energy status and activated by high AMP/ATP ratio to promote catabolism for energy-production.[22] In cancer cells, AMPK is usually found poorly expressed and opposes aerobic glycolysis (the Warburg effect).[19] The enhanced AMPK activity exhibits notable inhibitory effect on tumor growth.[19] One of the most important downstream effectors of AMPK is mammalian target of rapamycin (mTOR) signaling cascade. The activity of mTOR is negatively regulated by AMPK function, by which the energy variations monitored by AMPK is translated into the corresponding modulation of cellular activities.[23] As a renowned metabolic signaling participant, mTOR exerts its kinase function to promote a variety of gene transcriptions and protein biosyn-

*To whom correspondence should be addressed.
E-mail: xuyong1013@163.com (YX); xqh1126@sina.com (QX)

doi: 10.3164/jcbn.23-112

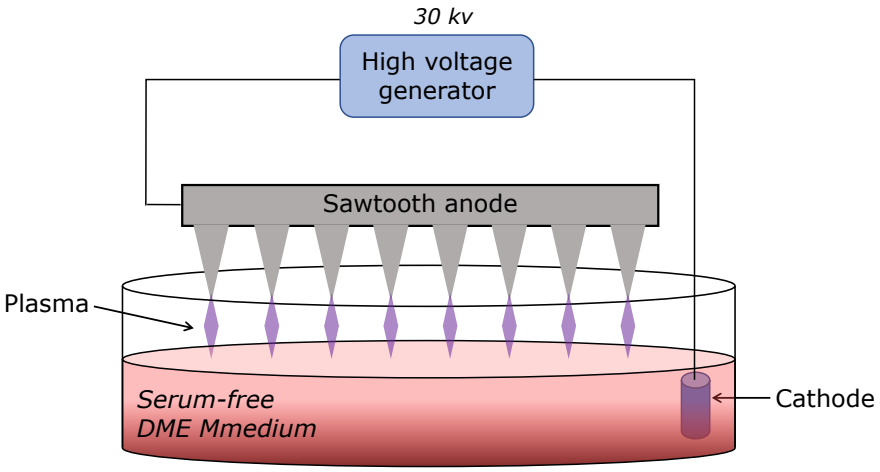


**Fig. 1.** The schematic diagram of the plasma device and the preparation of PAM.

thesis that are critical for cell proliferation and growth.[24] Abnormal up-regulation of mTOR has been found in multiple cancers including HCC, and demonstrated being associated with tumor development, poor prognosis and low survival ratio.[24,25] It has been observed that blockage of the salvage pathway in hepatocarcinoma cells triggered the suppressed AMPK kinase function, which in turn inhibits the activity of mTOR pathway and leads to impairment of cell growth and metabolism ultimately.[15]

Cold atmospheric plasma (CAP) is an emerging technology of generating plasma at room temperature and can be applied on temperature-sensitive substances. Recently, CAP is widely investigated in terms of biomedical application and found to be a novel agent against tumor cells.[26] In addition to direct CAP treatment, plasma-activated medium (PAM), being obtained by irradiation of cell-free medium with CAP, has been reported to kill tumor cells, HCC.[27–30] The anti-tumor effect of PAM is comparable with that of CAP but presents less cytotoxicity on normal cells, as such, PAM becomes a popular candidates for development of new targeted cancer therapy.[31] The mechanism underlying the tumor-specific inhibitory effect of PAM is still under investigation. To date, the best known cellular response to PAM is oxidative stress induced by the abundance of reactive oxygen and nitrogen species (RONS) in PAM, such as hydrogen peroxide ($H_2O_2$) and nitrate/nitrite ($NO_2^-$/$NO_3^-$).[32] As a potential consequence of PAM-induced oxidative stress, disruption of the mitochordrial function and ATP generation has been reported in several previous studies.[33,34] Being associated with this discovery, it was observed that an acute decrease in intracellular $NAD^+$ content occurred when PAM-treatments was applied on tumor cells, which hints at a dysfunction of the salvage pathway.[35] Taking all of these findings into account, the energy-metabolism system of tumor cells, particularly the salvage pathway, is presumed to be a fundamental target of the PAM-treatment to induce tumor-specific cytotoxicity. However, the direct experimental evidence to certify this inference and pinpoint the targets involved is still lacked.

Considering the reported selective inhibition of HCC cell lines by PAM, gaining a deeper insight into the mechanism of the anti-tumor effect of PAM would be of a great help to advance the clinic application of this novel agent for the HCC treatment. Therefore, in this study we investigated the PAM-induced alterations in the energy status of HCC cells, and made an effort to ascertain the detailed roles of the primary salvage pathway and its controlled AMPK/mTOR signaling in the PAM induced tumor-specific inhibition.

## Materials and Methods

**Cell culture.** HCC lines Huh7 and HepG2 and non-cancerous hepatocyte cell line HL-7702 were kept in our lab, were maintained in high glucose Dulbecco's modified Eagle's medium (DMEM; Cytiva, Logan, Utah), supplemented with 10% (v/v) fetal calf serum (ExCell Bio, Suzhou, China), 100 U/ml of penicillin and 0.1 mg/ml of streptomycin. All cells were cultured at 37°C in a humidified air with 5% $CO_2$.

**PAM preparation.** The discharge mode of CAP device in this study was atmospheric-pressure plasma jet (APPJ), which is a self-sustaining discharge in a gas operating under very low electric field.[36] The set up of APPJ device and the preparation of PAM were shown in Fig. 1. The working gas was air, and the discharge voltage was 30 kV. The positive electrode of the power supply was connected to the sawtooth anode, and the plasma plume was generated in the form of DC corona discharge at the tip of the anode. Firstly, 30 ml of high-glucose DMEM were added to a 100 ml staining jar. Then, the cathode was inserted into DMEM, and the positive electrode was covered on the staining jar. The exposure distance between the positive electrode tip and DMEM surface was kept at ~3 cm to avoid the generation of spark. In this study, the irradiation duration to prepare PAM was set as 5 min, 10 min, 15 min, and 20 min respectively, and the obtained PAMs were named PAM5, PAM10, PAM15, and PAM20 correspondingly. Finally, all PAMs were sterilized by filtration and supplemented with 10% FCS and antibiotics for cell treatments.

**Cell treatments.** NMN (Aladdin, Shanghai, China) was dissolved in PAMs or DMEM at the concentration of 100 mM as storage solution. In this study, cells were treated by PAMs or DMEM either with or without the supplementation of 500 μM NMN.

**Cell viability assay.** Huh-7, HepG2, and HL-7702 cells were seeded in a 96-well plate at $5 \times 10^3$ cells/well, respectively, and cultured to 80% confluence and then treated with different PAMs described above for 24 h. After treatments, PAMs were replaced by fresh complete DMEM medium, and the cell viability was determined using Cell Counting Kit-8 (CCK8; Beyotime, Shanghai, China) following the manufacturer's protocol to evaluate the potential toxic effects of PAMs on Huh-7, HepG2, and HL-7702 cells.


doi: 10.3164/jcbn.23-112

**Cell apoptosis assay.** Cell apoptosis were investigated by either staining phosphorylserine on cell membranes or determining intralcellular caspase 3/7 activity. Huh-7 cells were seeded in a 96-well plate at $1 \times 10^4$ cells/well, which is followed by treatments with PAMs or DMEM for 24 h. The treated cells have to be washed using phosphate-buffered saline (PBS) prior to cell apoptosis assays. The phosphorylserine on the cell membranes was stained using Annexin V-phycoerythrin Detection Kit (Beyotime) according to the manufacturer's protocol. The stained cells were observed under fluorescence microscope. The caspase 3/7 activities of cells were detected using caspase 3/7 assay kits (Sangon, Shanghai, China), where TF2-DEVD-FMK was used as a fluorescent indicator for the detection of caspase-3/7 activity. Once being bound to the caspases, the green fluorescent dye is retained inside cells. The fluorescence intensity was monitored at Ex/Em = 490/525 nm.

**Colony-formation assay.** Huh-7 cells were seeded in a 6-well plate at $1 \times 10^3$ cells/well and treated with PAMs and DMEM for 6 h, following which the treated cells were cultured in completed DMEM for 7 days. Sequentially, the cells were fixed with 3.7% formaldehyde and methanol for 20 min, and then stained with 0.05% crystal violet for 30 min. After being washed with PBS for 3 times, the images of the plate were acquired and the number of colonies were counted. Colony formation was calculated as (number of colonies formed under treatment/number of colonies formed by vehicle control group) × 100%.

**Mitochondrial membrane potential detection.** MitoTracker Red CMXRos (Beyotime) was used as probe to detect the mitochondrial membrane potential of cells. Huh-7 cells were seeded in a 96 well plate at $1 \times 10^4$ cells/well, and treated with PAMs and DMEM for 6 h. Afterwards, the cells were digested and centrifuged at 1,000 × *g* for 5 min to collect cell pellet. The cells were gently resuspended with the MitoTracker Red CMXRos working solution, and incubated at 37°C for 25 min. After incubation, the solution was centrifuged at 1,000 × *g* for 5 min. The obtained cell pellet was then resuspended using fresh cell culture medium at 37°C. The fluorescence of the Red CMXRos dye anchored to the mitochondrial membrane with normal potential was monitored at Ex/Em = 579/599 nm.

**Intracellular ATP assay.** The intracellular ATP level was measured using ATP Assay Kit (Beyotime), which is based on the fact that firefly luciferase (also known as luciferase) requires ATP to provide energy when it catalyzes luciferin to produce fluorescence. Approximate $10^6$ cells/well were seeded in a 6 well plate, and treated with PAM or DMEM for 6 h. In each well, 200 µl of lysate was added, and centrifuged at 4°C 12,000 *g* for 5 min to obtain the supernatant. Afterwards, ATP detection working solution was added, and fluorescent intensity was detected using Multimode Plate Reader (Molecular Devices, Sunnyvale, CA) at chemiluminescence mode.

**Determination of intracellular NAD.** Approximate $1 \times 10^6$ cells/well were seeded in a 6 well plate. Cells were treated with PAMs or DMEM for 6 h. Subsequently, intracellular NAD content was determined using $NAD^+$/NADH Assay Kit with WST-8 (Beyotime) following the manufacturer's protocol.

**Measurement of intracellular reactive oxygen species (ROS).** Huh-7 cells were seeded in a 96 well plate, and treated with PAM or DMEM for 6 h. Intracellular ROS level was detected using reactive oxygen species assay kit (Beyotime) following the manufacturers' protocols. The fluorescence probes DCFH-DA was used to detect ROS. The fluorescence intensity was detected at Ex/Em = 488/525 nm.

**Western blotting analysis.** Intracellular proteins of Huh-7 cells harvested after various treatment were extracted using cytoplasmic protein extraction kit (Biosharp, Beijing, China) were normalized to total protein amount in each sample. The extracted proteins were separated by 10% SDS-PAGE electrophoresis and then were transferred to polyvinylidene fluoride (PVDF) membrane by immunoimprinting electrophoresis. Afterwards, the target protein on the membrane was imprinted with the primary antibody anti-NAMPT and anti-NMNAT1 were purchased from (Signalway Antibody LLC, Greenbelt, MD), and anti-phospho-AMPKα (Thr172), anti-AMPKα, anti-phospho-mTOR (Ser2448), anti-mTOR, anti-phospho-p70S6K (Thr389), anti-p70S6K were purchased from Proteintech Group, Inc. (Wuhan, China). After washing three times using TBST (Tris-HCl buffer containing 0.1% Tween-20), the membranes were incubated with the anti-rabbit or anti-mouse IgG coupled with horseradish peroxidase (Promega, Madison, WI). Finally, the target protein was detected by TMB color reaction (Beyotime). β-actin was determined by immunoblotting as internal control to verify equivalent loading amounts of all samples. Densitometric quantification of Western blot was performed using Image J (NIH, Bethesda, MD).

**Expression and purification of NAMPT and NMNAT.** The gene encoding His tagged NAMPT or NMNAT was cloned and inserted into pcDNA3.1 to construct expression vector, which was subsequently transfected into Huh-7 cells for protein expression. The transfected cells were grown at 37°C for 24 h to allow the His tagged NAMPT or NMNAT expressing adequately. Afterwards, cells were treated with PAM or DMEM for 6 h, and then harvested and lysed. By taking advantage of a $Ni^{2+}$ mediated immobilized metal ion affinity chromatography, the recombinantly expressed NAMPT and NMNAT was isolated from the cell lysate. The concentration of isolated protein was determined using spectrophotometry.

**Measurement of NAMPT and NMNAT enzymatic activity.** The enzymatic activity of NAMPT was determined according to the method described by Zheng *et al.*[37] The reaction buffer for NAMPT catalysis was composed of 50 mM Tris-HCl (pH 7.5), 0.4 mM phosphoribosylpyrophosphate (PRPP; Sigma-Aldrich, St. Louis, MO), 2 mM ATP, 0.02% BSA, 2 mM dithiothreitol (DTT) and 10 mM $MgCl_2$. For each reaction, the purified NAMPT was added into 20 µl reaction buffer to dilute the enzyme concentration by $5 \times 10^{-2}$ µM. This buffer containing NAMPT was subsequently transferred into a well of a 96-well plate. All reactions were initiated by the addition of 0.2 mM NAM. After incubation at 37°C for 15 min, the NAMPT reaction was terminated by heating at 95°C for 1 min. To determine the yield of NMN in each reaction, 10 µl 20% acetophenone (dissolved by DMSO) and 10 µl 2 M KOH were added into the NAMPT reaction mixture in each well and storing in ice bath for 2 min. Afterwards, 45 µl 88% formic acid was added into mixture, and then incubated at 37°C for 10 min. Finally, 85 µl of the mixture was transferred into a black 96 well plate, and the fluorescence intensity was detected at Ex/Em = 382/445 nm. Background controls were set as the reaction mixture without NAM, and reference controls were set as the reaction catalyzed by the NAMPT without PAM treatments. The fluorescence intensity of sample ($F_S$) and the fluorescence intensity of reference controls ($F_R$) should be corrected by removing background fluorescence ($F_0$). Relative enzyme activity of NAMPT (activity%) was calculated according to the equation, Activity % = $[(F_S - F_0)/(F_R - F_0)] \times 100\%$.

The enzymatic activity of NMNAT was determined according to the method described by Haubrich *et al.*[38] In brief, each NMNAT catalysis reaction contains a 20 µl buffer consisting of 15 mM HEPES (pH 7.4), 20 mM NaCl, 10 mM $MgCl_2$, 1 mM EDTA, and 0.02% (v/v) Tween-20. 20 µM ATP and 100 µM NMN were applied as the substrates of NMNAT catalyzed reaction. Each reaction was initiated by the addition of the purified NMNAT with a final concentration of $2 \times 10^{-2}$ µM at 37°C. The reaction rate was detected by measuring the ATP consumption using luciferase-catalyzed fluorescence reaction.[38] The fluorescent intensity was detected using Multimode Plate Reader (Molecular Devices) at chemiluminescence mode.

**Detection of $H_2O_2$ and total nitrate/nitrite ($NO_3^-/NO_2^-$).** Huh-7 cells were seeded in a 96 well plate, and treated with PAM15 or DMEM for 6 h at 37°C. Intracellular $H_2O_2$ level was detected using Hydrogen Peroxide Assay Kit (Beyotime) according to the manufacturers' protocols. Xylenol orange was used in this assay to react with the $Fe^{3+}$ oxidized by the intracellular $H_2O_2$ and form a product with the specific absorbance at 560 nm.

Huh-7 cells were seeded in a 6 well plate, and treated with PAM15 or DMEM for 6 h at 37°C. Intracellular total $NO_3^-/NO_2^-$ was measured using Nitrate/Nitrite fluorometric Assay Kit (Cayman Chemical, Ann Arbor, MI) according to the manufacturers' instruction. The fluorescence intensity was detected at Ex/Em = 375/415 nm.

## Results

**PAM-treatment selectively inhibits the growth of HCC.** To determine the effect of PAM on hepatic cells, non-cancerous hepatocytes HL7702 and HCC Huh-7 and HepG2 cell lines were applied for comparison and incubated with regular DMEM medium, PAM5, PAM10, PAM15, PAM20 respectively for 12 h. As shown in (Fig. 2A), PAM-treatment only reduced the viability of Huh-7 and HepG2 cells but not affected HL7702 cells notably, which indicates a selective inhibitory effect of PAM on HCC cells. Within the dose range between PAM5 and PAM15, the specific cytotoxicity of PAM to Huh-7 became higher along with the increase of PAM dose (Fig. 2A). The PAM20 did not show more obvious effect on HCC cells than PAM15 (Fig. 2A). Further investigation unraveled that the treatment of PAM15 remarkably suppressed the colony formation of Huh-7, indicating the negative effect of the high dose PAM on cell proliferation (Fig. 2B). Meanwhile, a great amount of cell apoptosis was detected in the PAM-treated Huh-7 cells via either annexin V-phycoerythrin staining or measurement of caspase 3/7 (Fig. 2C and D). These observations exhibited a complexed cellular mechanism underlying the PAM cytotoxicity to Huh-7 cells.

**PAM-treatment induces intracellular oxidative stress and mitochondrial dysfunction.** Considering that the best characterized cellular effect of CAP is manipulating intracellular redox environment, the ROS level inside the PAM-treated Huh-7 cells was examined to assess the association between the PAM-induced redox status and the PAM tumor-specific cytotoxicity. The result of intracellular ROS assays demonstrated that the ROS level of the Huh-7 cells grown in PAM was almost double of that of the cells without PAM-treatment (Fig. 3A), suggesting a superoxidized intracellular environment. To inspect whether the high ROS level leads to oxidative damage to mitochondria, the mitochondrial membrane potential, as an indicator of the integrity of mitochondrial function, was determined for the Huh-7 cells either with or without PAM-treatment. Compared with that of the PAM-absence group, the fluorescence intensity of PAM-exposed Huh-7 cells was significantly decreased (Fig. 3B), which confirmed that disrupted mitochondrial membrane potential and a dysfunction of respiratory chain were resulted by PAM-exposure. Loss of mitochondrial membrane potential commonly plays a considerable role in the energy metabolism failure and cell apoptosis. Accordingly, the ATP level detected in the PAM-treated Huh-7 cells was significantly lower than that in untreated cells, demonstrating a energy depletion under the effect of PAM (Fig. 3C).

**The disruption of the salvage pathway and NAMPT significantly contributes to the PAM-effect on Huh-7 cells.** Previous studies on a range of tumor cell types reveal an association between the diminishing of intracellular $NAD^+$ and devastation of the respiratory chain. To ascertain whether loss of $NAD^+$ occurs as well as the disruption of the respiratory chain induced by PAM in HCC, the content of total NAD, including $NAD^+$ and NADH, in the PAM-treated Huh-7 cells was determined. The obtained data showed a distinct reduction in the yield of NAD (Fig. 4A). When Huh-7 cells was subject to PAM15, the amount of intracellular NAD dropped almost by half compared with that of the untreated cells (Fig. 4A).

As aforementioned, the salvage pathway plays a predominant role in the generation of $NAD^+$ in HCC and is a critical constituent of the energy production system. This property hints at the salvage pathway as a probable target responding to the PAM-effect to interrupt the synthesis of $NAD^+$ in Huh-7 cells. To assess this hypothesis, a series of PAM-treatments on Huh-7 cells were carried out in the presence or absence of NMN, which is followed by the measurement of the intracellular NAD level, including both $NAD^+$ and NADH contents. NMN is synthesized by NAMPT catalysis and is the sole substrate for the $NAD^+$ production in the salvage pathway. In theory, if the addition of NMN restores the $NAD^+$ supply, PAM-effect should influence NMAPT or its upstream enzymes, contrariwise NMNAT would be identified as the unique target of PAM-effect in the salvage pathway. As a result, compared with the singly PAM-treated group, the addition of NMN effectively counteracted the depletion of $NAD^+$ caused by PAM-treatment, increasing the NAD content to the similar level of that in non-treated cells (Fig. 4A). Correspondingly, the presence of NMN rescued Huh-7 cells from the PAM-induced cytotoxicity to a notable extent (Fig. 4B). It worth noting that in the absence of PAM-effect the addition of NMN did not promote the $NAD^+$ generation and cell proliferation of Huh-7 cells. We reasoned that the substantially high $NAD^+$ turnover inside HCC to meet the cells' great demand for energy is likely to exploit NAMPT and NMNAT catalytic capacities to the utmost extent already, which results in the supplemented NMN can not be utilized notably.

These observations indicate that NAMPT, but not NMNAT is seemingly the primary target of PAM-effect in HCC, so the changes in the expressions and activities of NAMPT and NMNAT under the effect of PAM were detected respectively, as to clarify the roles of NAMPT and NMNAT. The NAMPT expression level was examined using Western blot (WB), which exhibited little change under the effect of PAM (Fig. 4C). Subsequently, the NAMPT enzymes expressed in the Huh-7 cells with and without PAM-treatment were isolated separately and then subjected to enzymatic assays. It was observed that in the presence of PAM-effect the NAMPT activity was obviously decreased compared with that from the non-treated cells (Fig. 4D). In contrast, neither expression level nor enzymatic activity of NMNAT exhibited significant change following the PAM-treatment (Fig. 4E and F). Based on these results, it is deduced that PAM-effect indeed targets on NAMPT and down-regulates the enzyme's activity. NAMPT and its catalyzed NMN synthesis play a crucial role in the response to PAM caused energy depletion.

**The effect of main long-lived RONS species on NAMPT enzymatic function.** To clarify the association of the superoxidized intracellular environment with the unefficient NAMPT function under PAM-effect, enzymatic activities of the purified NAMPT pre-treated by a buffer (25 mM Tris-Cl, pH 8.0, 150 mM NaCl, 0.02% BSA, and 10 mM $MgCl_2$) containing the main long-lived RONS species (RONS-buffer), including $H_2O_2$, $NO_2^-$, and $NO_3^-$, were examined *in vitro*. Concentrations of the RONS species were adjusted to 6 μM for $H_2O_2$, 18 μM for $NO_2^-$, and 18 μM for $NO_3^-$ referring to the intracellular concentrations of $H_2O_2$ and total nitrate/nitrite of the Huh-7 cells treated by PAM which are much higher than those inside the untreated cells (Fig. 5A). NAMPT was treated with the RONS-buffer for 4 h prior to being subjected to enzymatic assays. Resultantly, the enzymatic activity of NAMPT was declined by ~20% under the treatment of RONS-buffer (Fig. 5B), not as much as what observed for the NMAPT isolated from PAM treated cells. This


doi: 10.3164/jcbn.23-112

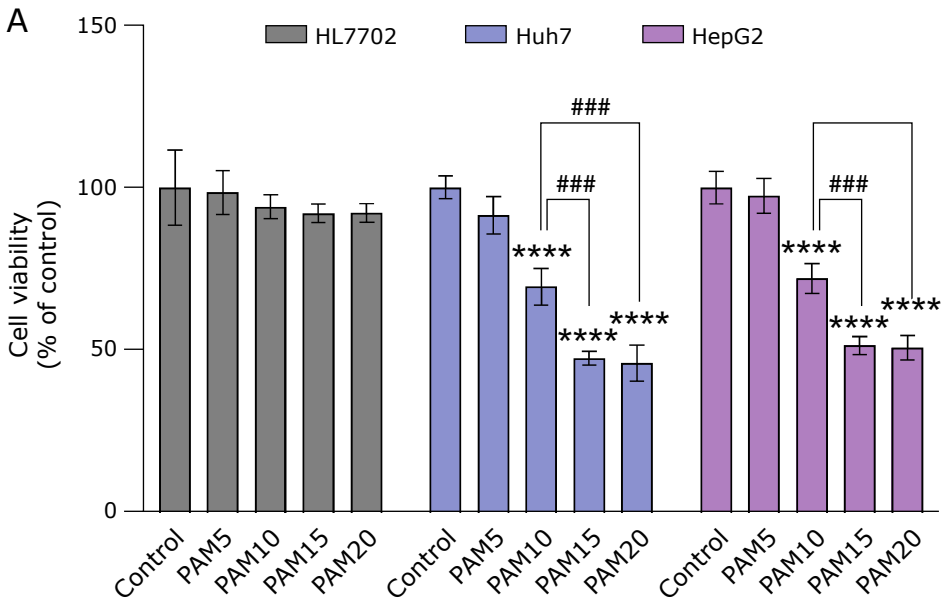


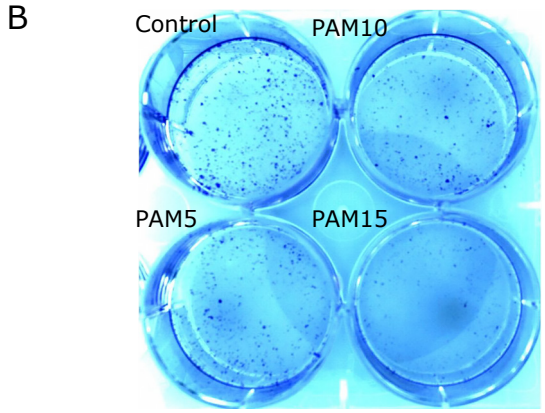


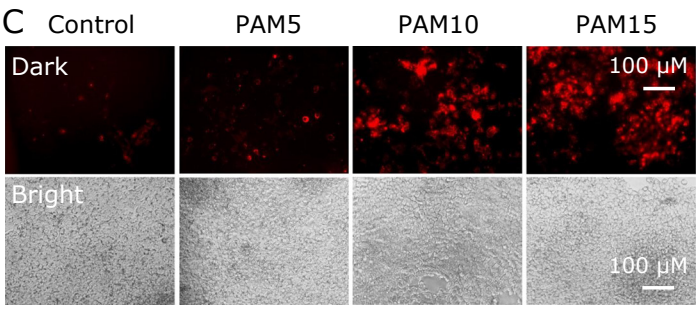


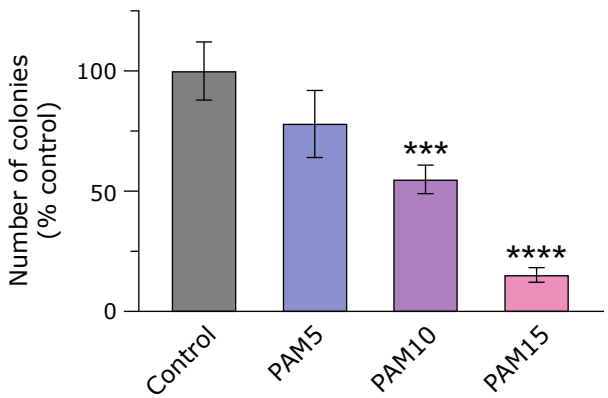


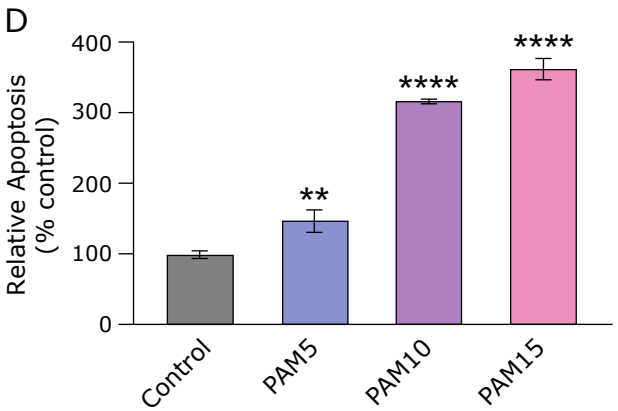


**Fig. 2.** The tumor-specific inhibitory effect of PAM on the HCC. (A) non-cancerous hepatocyte cell line HL7702, or HCC cell lines Huh-7 or HepG2 were treated with normal DMEM medium (control), PAM5, PAM10, PAM15, and PAM20 for 24 h respectively. Thereafter, cell viability was measured using CCK8 assay. The relative viability was calculated as the ratio of the viability of PAM-treated to control cells. (B) The upper panel shows the colony-formation ability of Huh7 cells exposed to different media as indicated for 7 days; the lower panel shows the quantification of colony-formation data. (C) After 24 h exposure to different PAM as the indicated, apoptotic Huh-7 cells were stained by annexin V-phycoerythrin and observed under fluorescence microscopy (scale bar: 100 μm). (D) The quantification of apoptosis of Huh-7 cells exposed to different PAM through detecting caspase 3/7 using TF2-DEVD-FMK fluorescent indicator. The fluorescent intensities were monitored, and the relative apoptosis was calculated as the ratio of the fluorescent intensities of PAM-treated to control cells. All data are presented as means ± SD of three independent experiments. $^{**}p<0.01$, $^{***}p<0.001$, $^{****}p<0.0001$ compared to control; $^{\#\#\#}p<0.001$.

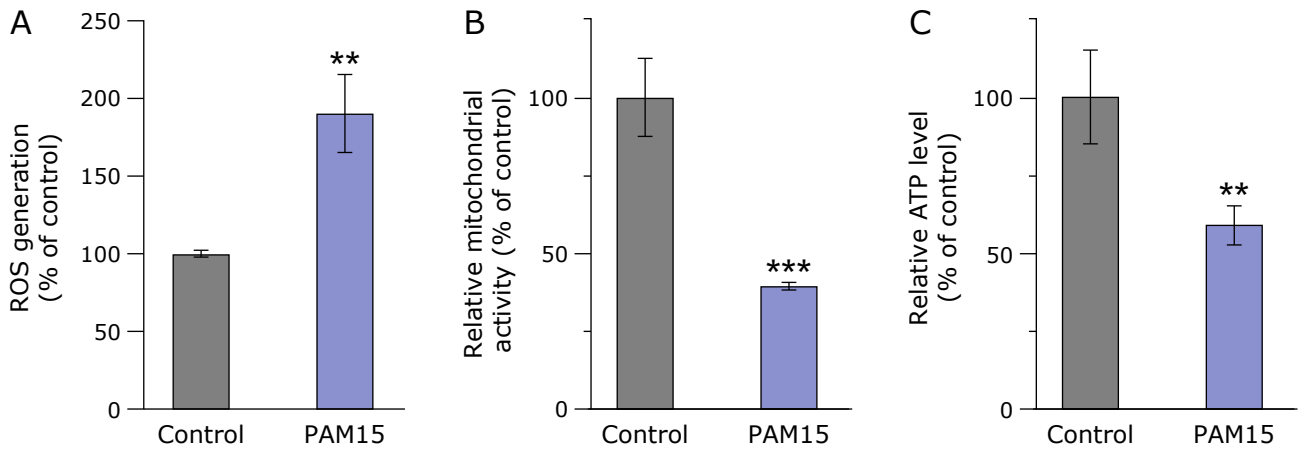


**Fig. 3.** The induction of oxidative stress and mitochondrial dysfunction by PAM. (A) The relative ROS generation of Huh-7 cells exposed to either normal DMEM (control) or PAM15 for 6 h. The intracellular ROS content was detected using fluorescence probe DCFH-DA. The relative ROS generation was calculated as the ratio of the fluorescence intensities of PAM-treated to control cells. (B) The relative mitochondrial activity of Huh-7 cells exposed to either normal DMEM (control) or PAM15 for 6 h. The mitochondrial membrane potential was detected using fluorescence probe CMXRos. The relative mitochondrial activity was calculated as the ratio of the fluorescence intensities of PAM-treated to control cells. (C) The relative ATP level of Huh-7 cells exposed to either normal DMEM (control) or PAM15 for 6 h. The ATP content was detected using luciferase-catalyzed bioluminescence assay. The relative ATP level was calculated as the ratio of the bioluminescence of PAM-treated to control cells. All data are presented as means ± SD of three independent experiments. $^{**}p<0.01$, $^{***}p<0.001$ compared to control.

result indicates that these long-lived RONS species are likely involved in the disruption of NAMPT activity by PAM-treatment but do not exert the major effect by themselves.

**PAM-induced depletion of $NAD^+$ activates AMPKα and suppresses the mTOR pathway in Huh-7 cells.** AMPKα-mTOR signaling axis functions as an important effector regulating protein synthesis and cell growth responding to cellular energy variations. To assess the effect of PAM-caused $NAD^+$ reduction on AMPKα-mTOR axis in Huh-7, the expression and phosphorylation levels of AMPKα, mTOR, and 70S ribosomal protein S6 kinase (p70S6K) were determined. p70S6K is one of the mTOR's substrate-kinases. Under the effect of PAM, the expression of all the three kinases in Huh-7 cells did not show observable change (Fig. 6). However, the phosphorylation of AMPKα at Thr172 was enhanced by PAM-treatment (Fig. 6), and accordingly the phosphorylations of mTOR at Ser2448 and p70S6K at Thr389 were both significantly down-regulated, indicating the activation of AMPKα and the inhibition of mTOR pathway (Fig. 6). Intriguingly, when NMN was supplemented in the PAM-treatment, the phosphorylation status of AMPKα, mTOR, and p70S6K induced by PAM-effect were all reversed, back to their original levels (Fig. 6). This finding reveals that the modulation of AMPKα-mTOR axis is a downstream event of the variation of $NAD^+$ levels induced by PAM-effect in Huh-7 cells. Therefore, the NAMPT enzymatic function should be extensively involved in the regulation of AMPKα-mTOR signaling axis by PAM-effect.

## Discussion

Lack of effective therapeutic tools and poor prognosis considerably increase the difficulty of treatment of HCC, and make it urgent to seek for new agents with low side-effect to fight against this notorious disease. The recent advancement of CAP technique and its reported tumor-killing effect inspire researchers to exploit the CAP potential in clinic cancer therapy.[30,39] Direct irradiation is the conventional way of CAP treatment, besides which, lately CAP is applied to generate PAM which then exerts the biological effect of plasma in a direct way.[40] Previous studies on PAM-effect on several tumor cells exhibited the outstanding advantage of PAM-treatment, that is, inhibiting tumor cells exclusively with little cytotoxicity on normal cells.[31,41,42] With respect to HCC, Li *et al.*[43] reported that the PAM was able to discriminated HCC cell line Hep3B from normal cell line MIHA and exerted inhibitory effect on the carcinoma cells. In our study, we chose HCC cell lines Huh-7 and HepG2 and normal hepatic cell line HL7702 as materials for examining how the presence of PAM affects cellular viability. As a consequence, we observed a serious cell death of Huh-7 in contrast to the insignificantly affected growth of HL7702 (Fig. 2A), which is consistent to previous finding. Based on our observation, PAM-treatment impairs the viability of Huh-7 cells through both interrupting cell proliferation and inducing apoptosis, presenting a complexed anti-tumor effect (Fig. 2B–D).

Up to dated, the understanding of mechanism underlying the PAM-induced cell death have focused on the intracellular oxidative stress and its resulted mitochondrial dysfunction.[33,34,44] According to the available research data, the presence of PAM disrupts the mitochondrial redox balance via promoting the yield of intracellular RONS, which in turn profoundly decreases the $NAD^+$ and ATP levels and induces apoptosis.[35] In accordance with these findings, our investigation demonstrates significant increases of ROS level in Huh-7 cells under the effect of PAM (Fig. 3A). In companion with the oxidative stress, the mitochondrial potential of PAM-treated Huh-7 cells was disordered and the ATP was depleted, suggesting a dysfunctional respiratory chain (Fig. 3C and D). Such a disruption in energy supply is lethal to HCC cells. However, the detailed mechanisms translating oxidative stress to the dysfunction of respiratory chain still remains unclear. Based on previous researches and our current study, we thought that the loss of $NAD^+$, another dramatic response of HCC to PAM (Fig. 4A), could be the key pieces to crack this puzzle.

As aforementioned, anoxic microenvironment adapts solid tumors to employ glycolysis as the sole energy origin to provide NADH for the normal function of respiratory chain.[45] The deficiency in $NAD^+$ directly results in the NADH depletion that further obstructs respiratory chain.[35,45] Therefore, as the only $NAD^+$ supplier in HCC, the salvage pathway and its component enzymes, such as NAMPT and NMNAT, are the most potential


doi: 10.3164/jcbn.23-112

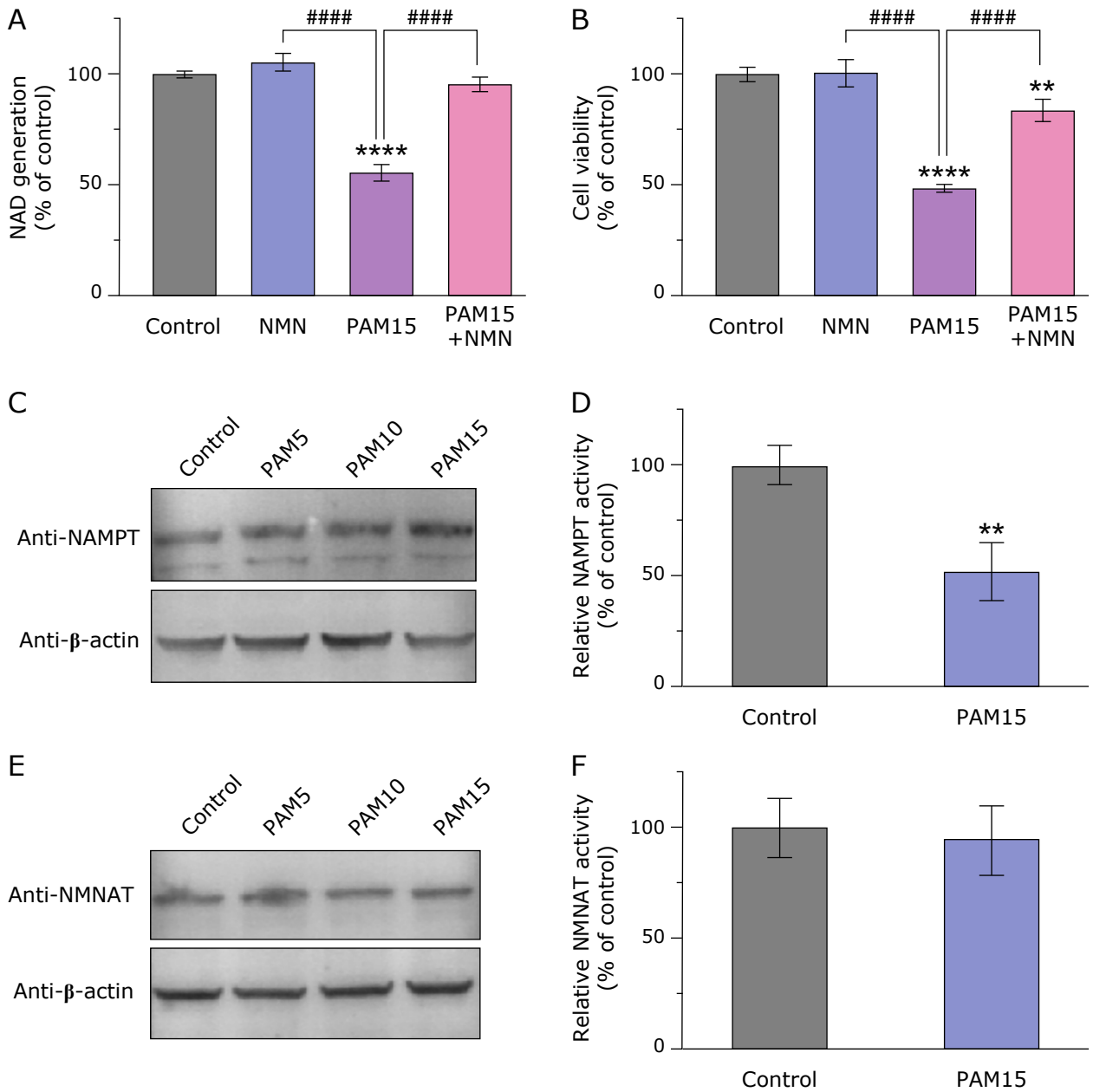


**Fig. 4.** The reductions in NAD synthesis and NAMPT activity caused by PAM-effect. The relative NAD generation level (A) and cell viability (B) of Huh-7 cells exposed to normal DMEM (control) or PAM15 in the either presence or absence of NMN (500 μM). The intracellular NAD content was detected using spectrophotometry, and the relative NAD generation was calculated as the ratio of the absorbance at 450 nm of PAM-treated to control cells. (C) Western blot analysis of expression level of NAMPT (C) and NMNAT (E) in Huh-7 cells treated with normal DMEM (control), PAM5, PAM10, and PAM15 for 24 h. β-Actin was used as loading control. (D) The relative activity of recombinantly expressed NAMPT (D) and NMNAT (F) in the Huh-7 cells exposed to normal DMEM (control) or PAM15 for 6 h. The relative enzymatic activity was calculated as the ratio of the product-yield rates of PAM-treated to control groups. All data are presented as means ± SD of three independent experiments. $^{**}p<0.01$, $^{****}p<0.0001$ compared to control; $^{\#\#\#\#}p<0.0001$.

effectors responding to the PAM-caused oxidative stress.[33,35] In our study, the regulation of NAMPT and NMNAT by PAM-treatment was investigated. The results did not show any significant effect of PAM on both the expression and activity of NMNAT (Fig. 4E and F). However, the presence of PAM remarkably weakened the enzymatic activity of NAMPT to convert NAM to NMN in spite of little change in the expression level of the enzyme (Fig. 4C). *In vitro* assay for detecting the effect of the mixture including $H_2O_2$, $NO_2^-$, and $NO_3^-$ on NAMPT indicates long-lived RONS is able to influence NAMPT activity but not remarkable (Fig. 5B). Despite of this, the impact of RONS upon NAMPT and the salvage pathway can not be underestimated hastily yet, considering that the long-lived RONS only accounts for a part of the complexed RONS system arising from PAM-treatment, and different RONS components potentially produce synergistic effects.[46] However, the composition and content of RONS induced by PAM-effect has not been completely unraveled so far, which causes a huge trouble in reconstruction of the RONS system *in vitro* for mimicing the effect of the intracellular oxidative stress on NAMPT. To tackle

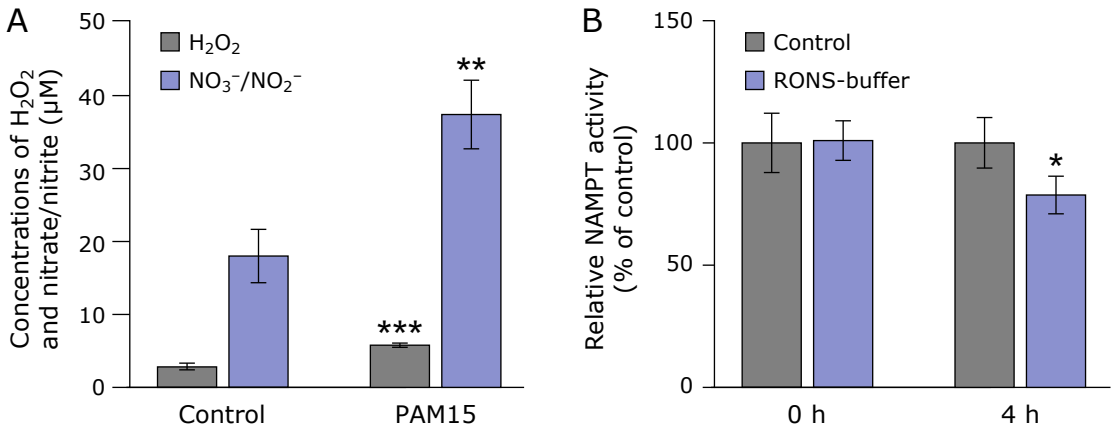


**Fig. 5.** The effect of main long-live RONS species ($H_2O_2$ and $NO_3^-/NO_2^-$) on the activity of NAMPT. (A) The intracellular concentrations of $H_2O_2$ and $NO_3^-/NO_2^-$ of Huh-7 cells exposed to either normal DMEM (control) or PAM15 for 6 h. (B) The relative NAMPT activity exposed to a buffer either without or with $H_2O_2$ and $NO_3^-/NO_2^-$ (control or RONS-buffer). The purified NAMPT was pre-treated by control or RONS-buffer for 0 h and 4 h at 23°C, which was followed by a buffer exchange of the treated enzyme to the reaction buffer to determine the enzymatic activity. The relative enzymatic activity was calculated as the ratio of product-yield rates of the RONS-buffer treated to control groups. All data are presented as means ± SD of three independent experiments. *$p$<0.05, **$p$<0.01, ***$p$<0.001 compared to control.

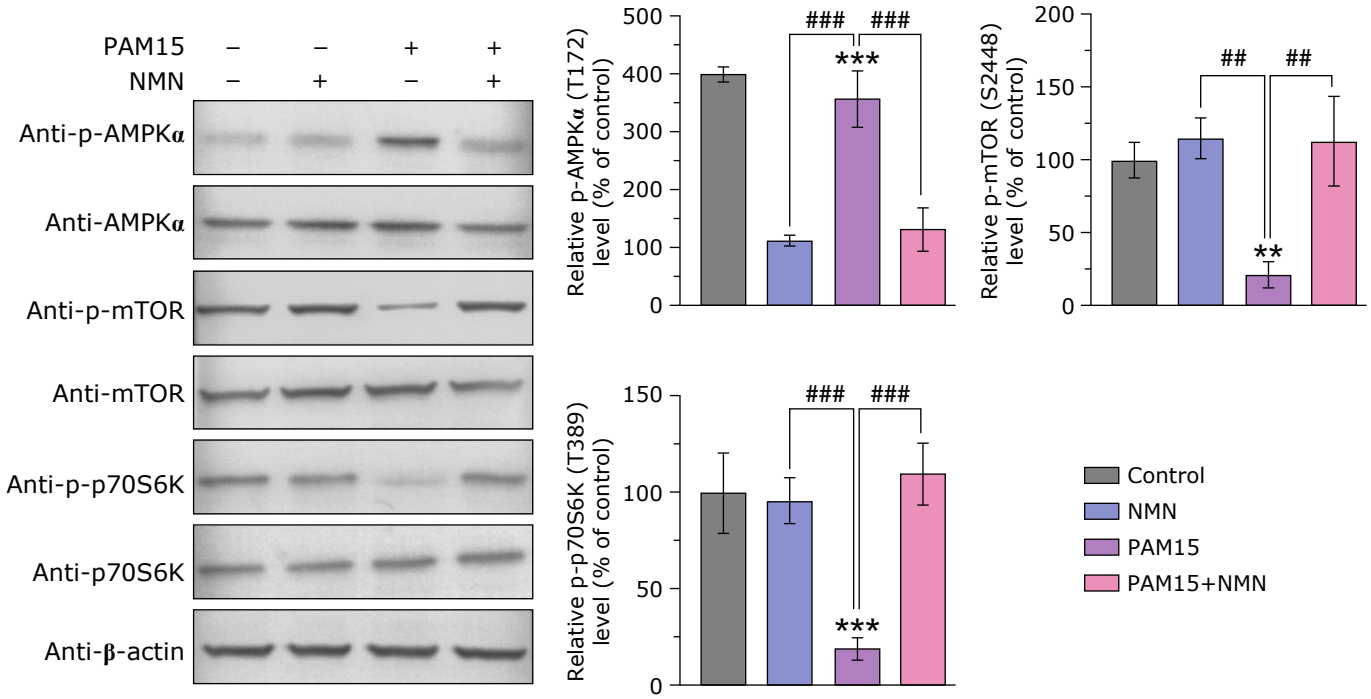


**Fig. 6.** The regulation of PAM-effect on AMPKα and mTOR pathway in Huh-7 cells. Western blot analysis of AMPK and mTOR expression and phosphorylation status in Huh7 cells treated with normal DMEM (control) or PAM15 in the either presence or absence of NMN (500 μM) for 24 h. β-Actin was used as loading control. All data are presented as means ± SD of three independent experiments. **$p$<0.01, ***$p$<0.001 compared to control; ##$p$<0.01, ###$p$<0.001.

this issue, further investigations are underway. Moreover, the addition of NMN in the PAM-treatment so as to compensate for the inefficacy of NAMPT activity increased the NAD yield close to the normal level, and profoundly rescued the Huh-7 cell from the cytotoxicity of PAM (Fig. 4A). Being combined with the results of enzymatic assays, this finding suggests that down-regulation of NAMPT activity is a major consequence of PAM-treatment on Huh-7 cells, which plays an essential part in the blockage of the salvage pathway and the loss of $NAD^+$ induced by PAM-effect. In contrast to HCC cells, non-cancerous hepatocytes can employ all three $NAD^+$ synthesis pathways and generate energy via both glycolysis and oxidative phosphorylation, hence, the salvage pathway is dispensable and the loss of NAMPT function could not be fatal for normal hepatocytes.[47] To a certain extent, the susceptibility of NAMPT to PAM-effect determines that PAM-treatment imposes considerable inhibitory


doi: 10.3164/jcbn.23-112

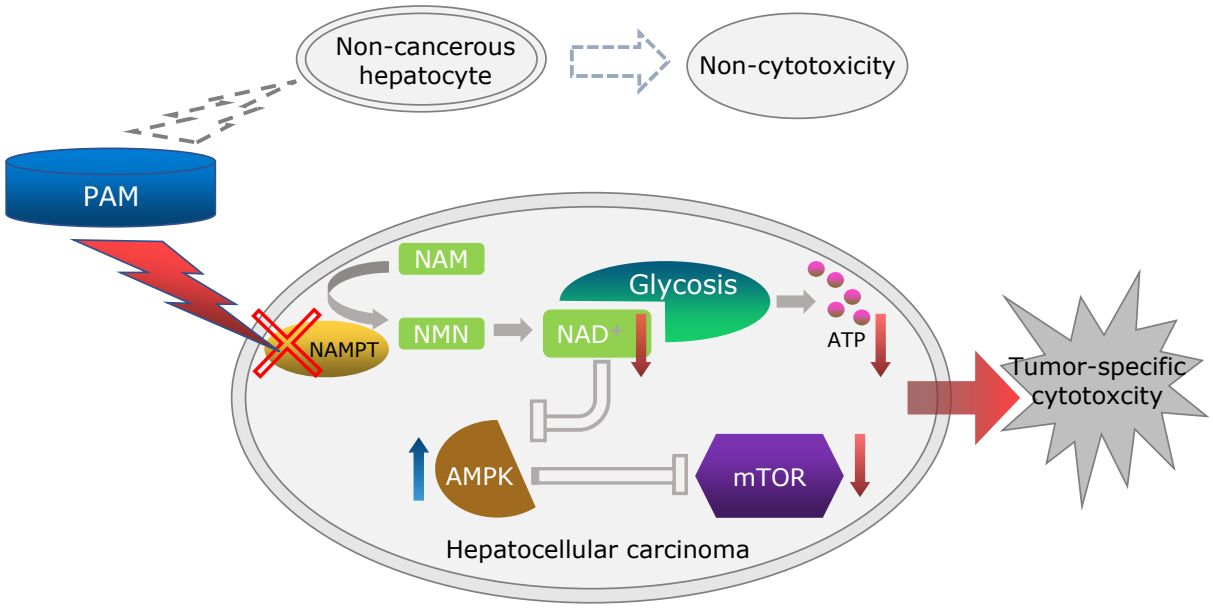


**Fig. 7.** The schematic illustrating the mechanism underlying the PAM-specific cytotoxicity unraveled in this study.

effect on HCC rather than normal hepatocytes.

In parallel with the energy failure in Huh-7 cells due to the PAM-induced NAMPT's dysfunction, the activity of AMPK-mTOR signaling axis was significantly modulated according to our observation. This modulation presents a significant increase in AMPK activity and a consequent inhibition of mTOR and its downstream kinases, such as p70S6K (Fig. 6). Suppressed AMPK and activated mTOR pathway has been reported in several human cancer cells including HCC, which contributes to the abnormally rapid proliferation and growth state of carcinoma cells.[15,19,23,24] Therefore, it is reasonable to consider manipulation of AMPK-mTOR pathway as one of the means whereby the effect of PAM suppresses the cell growth of HCC. Intriguingly, the presence of NMN in the PAM-treatment counteracted the effect of PAM singly on AMPKα-mTOR axis, leading to a drop in AMPK activity and a bounce in mTOR activity. This combinatorial effect of NMN and PAM implicates that the modulation of AMPK-mTOR axis is a downstream event following the impairment of NAMPT activity by PAM-treatment. Hence, we infer that the AMPK-mTOR axis of HCC is able to sense and respond to the energy metabolic signal generated by the salvage pathway to inhibit cell growth and metabolism. Taking the inhibitory effect of AMPK on aerobic glycolysis into account, the up-regulation of AMPK induced by the disruption of the salvage pathway may further interrupt the energy metabolism of PAM-treated HCC in a feedback manner.

All in all, our study confirmed that PAM-treatment exerts specific cellular toxicity on hepatocarcinoma cells rather than normal cells. Cellular investigations revealed that the oxidative stress induced by PAM-treatment led to the mitochondrial dysfunction and energy depletion in HCC. On the basis of this PAM-effect on the energy metabolism, the salvage pathway and its key component enzyme NAMPT were further unraveled as crucial targets of PAM to discriminate HCC from normal cells and thereby inhibit the energy production. In addition to the shortage of energy, the PAM caused blockage of the salvage pathway triggers the activation of AMPKα and suppression of mTOR pathways, resulting in a reinforced cell growth inhibition. These findings provide a deeper insight into the mechanism underpinning the tumor-specific inhibition by PAM-treatment (Fig. 7). Only with a better understanding of the treatment targets, it is possible to modify PAM purposely to advance its clinic application in the future.

## Author Contributions

Conceptualization, YX and QX; writing—original draft preparation, YB; methodology, YB and YX; investigation, YB, YX, NC, CD, XZ, and HL; writing—review & editing, YX, CD, and XZ; funding acquisition, YB and QX. All authors have read and agreed to the published version of the manuscript.

## Acknowledgments

This research was funded by a grant from a key program of the SCIENTIFIC RESEARCH PROGRAM OF HIGHER EDUCATION INSTITUTIONS OF ANHUI PROVINCE in 2023 (No. 2023AH052602). This research was also supported by a key program of the HEALTH RESEARCH PROGRAM OF ANHUI PROVINCE in 2022 (No. AHWJ2022a006). We would like to thank Yonghong Wu for design of APPJ device.

## Abbreviations

| | |
|---|---|
| AMPK | AMP-activated protein kinase |
| APPJ | atmospheric-pressure plasma jet |
| CAP | cold atmospheric plasma |
| HCC | hepatocellular carcinoma |
| mTOR | mammalian target of rapamycin |
| $NAD^+$ | nicotinamide adenine dinucleotide |
| NAM | nicotinamide |
| NAMPT | nicotinamide phosphoribosyl transferase |
| NMNAT | nicotinamide mononucleotide adenylyltransferase |
| PAM | plasma-activated medium |
| p70S6K | protein S6 kinase |
| RONS | reactive oxygen species and reactive nitrogen species |
| ROS | reactive oxygen species |

## Data Availability Statement

The data that support the findings of this study are available from the corresponding author upon reasonable request.

## Conflict of Interest

No potential conflicts of interest were disclosed.

## References


1 Gao Y, Li W, Liu R, *et al*. Norcantharidin inhibits IL-6-induced epithelial-mesenchymal transition via the JAK2/STAT3/TWIST signaling pathway in hepatocellular carcinoma cells. *Oncol Rep* 2017; **38**: 1224–1232.
2 Blum HE. Hepatocellular carcinoma: HCC. *Hepat Mon* 2011; **11**: 69–70.
3 Heller M, Parikh ND, Fidelman N, Owen D. Frontiers of therapy for hepatocellular carcinoma. *Abdom Radiol (NY)* 2021; **46**: 3648–3659.
4 Wang Y, Li M, Yu X, *et al*. Sinomenine hydrochloride inhibits cell survival in human hepatoma Huh7 cells. *Biomed Rep* 2018; **8**: 510–516.
5 Khan HY, Maurya SK, Siddique HR, Yousuf S, Arjmand F. New tailored RNA-targeted organometallic drug candidates against Huh7 (Liver) and Du145 (Prostate) cancer cell lines. *ACS Omega* 2020; **5**: 15218–15228.
6 DeWaal D, Nogueira V, Terry AR, *et al*. Hexokinase-2 depletion inhibits glycolysis and induces oxidative phosphorylation in hepatocellular carcinoma and sensitizes to metformin. *Nat Commun* 2018; **9**: 446.
7 Warburg O. On the origin of cancer cells. *Science* 1956; **123**: 309–314.
8 Cha YH, Yook JI, Kim HS, Kim NH. Catabolic metabolism during cancer EMT. *Arch Pharm Res* 2015; **38**: 313–320.
9 Lin Y, Wei X, Jian Z, Zhang X. METTL3 expression is associated with glycolysis metabolism and sensitivity to glycolytic stress in hepatocellular carcinoma. *Cancer Med* 2020; **9**: 2859–2867.
10 Xiao Y, Elkins K, Durieux JK, *et al*. Dependence of tumor cell lines and patient-derived tumors on the NAD salvage pathway renders them sensitive to *NAMPT* inhibition with GNE-618. *Neoplasia* 2013; **15**: 1137–1146.
11 Shames DS, Elkins K, Walter K, *et al*. Loss of NAPRT1 expression by tumor-specific promoter methylation provides a novel predictive biomarker for NAMPT inhibitors. *Clin Cancer Res* 2013; **19**: 6912–6923.
12 Chiarugi A, Dölle C, Felici R, Ziegler M. The NAD metabolome—a key determinant of cancer cell biology. *Nat Rev Cancer* 2012; **12**: 741–752.
13 Nikiforov A, Dölle C, Niere M, Ziegler M. Pathways and subcellular compartmentation of NAD biosynthesis in human cells: from entry of extracellular precursors to mitochondrial NAD generation. *J Biol Chem* 2011; **286**: 21767–21778.
14 Sharif T, Ahn DG, Liu RZ, *et al*. The $NAD^+$ salvage pathway modulates cancer cell viability via p73. *Cell Death Differ* 2016; **23**: 669–680.
15 Schuster S, Penke M, Gorski T, *et al*. FK866-induced NAMPT inhibition activates AMPK and downregulates mTOR signaling in hepatocarcinoma cells. *Biochem Biophys Res Commun* 2015; **458**: 334–340.
16 Garten A, Schuster S, Penke M. Could NAMPT inhibition become a potential treatment option in hepatocellular carcinoma? *Expert Rev Anticancer Ther* 2017; **17**: 289–291.
17 Navas LE, Carnero A. Nicotinamide adenine dinucleotide (NAD) metabolism as a relevant target in cancer. *Cells* 2022; **11**: 2627.
18 Revollo JR, Grimm AA, Imai S. The NAD biosynthesis pathway mediated by nicotinamide phosphoribosyltransferase regulates Sir2 activity in mammalian cells. *J Biol Chem* 2004; **279**: 50754–50763.
19 Schuster S, Penke M, Gorski T, *et al*. Resveratrol differentially regulates NAMPT and SIRT1 in hepatocarcinoma cells and primary human hepatocytes. *PLoS One* 2014; **9**: e91045.
20 Espindola-Netto JM, Chini CCS, Tarragó M, *et al*. Preclinical efficacy of the novel competitive NAMPT inhibitor STF-118804 in pancreatic cancer. *Oncotarget* 2017; **8**: 85054–85067.
21 Chauhan AS, Liu X, Jing J, *et al*. STIM2 interacts with AMPK and regulates calcium-induced AMPK activation. *FASEB J* 2019; **33**: 2957–2970.
22 Choi SL, Kim SJ, Lee KT, *et al*. The regulation of AMP-activated protein kinase by $H_2O_2$. *Biochem Biophys Res Commun* 2001; **287**: 92–97.
23 Cheng JD, Huang TL, Li YF, *et al*. AMP-activated protein kinase suppresses the *in vitro* and *in vivo* proliferation of hepatocellular carcinoma. *PLoS One* 2014; **9**: e93256.
24 Saxton RA, Sabatini DM. mTOR signaling in growth, metabolism, and disease. *Cell* 2017; **168**: 960–976.
25 Zhou L, Huang Y, Li J, Wang Z. The mTOR pathway is associated with the poor prognosis of human hepatocellular carcinoma. *Med Oncol* 2010; **27**: 255–261.
26 Muhammad AI, Xiang Q, Liao X, Liu D, Ding T. Understanding the impact of nonthermal plasma on food constituents and microstructure—a review. *Food Bioprocess Technol* 2018; **11**: 463–486.
27 Yoshikawa N, Liu W, Nakamura K, *et al*. Plasma-activated medium promotes autophagic cell death along with alteration of the mTOR pathway. *Sci Rep* 2020; **10**: 1614.
28 Keidar M. A prospectus on innovations in the plasma treatment of cancer. *Phys Plasmas* 2018; **25**: 083504.
29 Partecke LI, Evert K, Haugk J, *et al*. Tissue tolerable plasma (TTP) induces apoptosis in pancreatic cancer cells *in vitro* and *in vivo*. *Bmc Cancer* 2012; **12**: 473.
30 Lin L, Ding CB, Jin T, *et al*. A meaningful attempt: applying dielectric barrier discharge plasma to induce apoptosis of MDA-MB-231 cells via regulating *HIF-1α*/*VEGFA* expression. *Surf Coat Technol* 2020; **401**: 126293.
31 Jo A, Joh HM, Chung TH, Chung JW. Anticancer effects of plasma-activated medium produced by a microwave-excited atmospheric pressure argon plasma jet. *Oxid Med Cell Longev* 2020; **2020**: 4205640.
32 Ikeda JI, Tanaka H, Ishikawa K, Sakakita H, Ikehara Y, Hori M. Plasma-activated medium (PAM) kills human cancer-initiating cells. *Pathol Int* 2018; **68**: 23–30.
33 Nagaya M, Hara H, Kamiya T, Adachi T. Inhibition of NAMPT markedly enhances plasma-activated medium-induced cell death in human breast cancer MDA-MB-231 cells. *Arch Biochem Biophys* 2019; **676**: 108155.
34 Adachi T, Tanaka H, Nonomura S, Hara H, Kondo S, Hori M. Plasma-activated medium induces A549 cell injury via a spiral apoptotic cascade involving the mitochondrial-nuclear network. *Free Radic Biol Med* 2015; **79**: 28–44.
35 Kurake N, Ishikawa K, Tanaka H, *et al*. Non-thermal plasma-activated medium modified metabolomic profiles in the glycolysis of U251SP glioblastoma. *Arch Biochem Biophys* 2019; **662**: 83–92.
36 Xu Y, Bai Y, Dai CW, Lv H, Zhou XH, Xu QH. Effects of non-thermal atmospheric plasma on protein. *J Clin Biochem Nutr* 2022; **71**: 173–184.
37 Zheng XZ, Bauer P, Baumeister T, *et al*. Structure-based identification of ureas as novel nicotinamide phosphoribosyltransferase (Nampt) inhibitors. *J Med Chem* 2013; **56**: 4921–4937.
38 Haubrich BA, Ramesha C, Swinney DC. Development of a bioluminescent high-throughput screening assay for nicotinamide mononucleotide adenylyltransferase (NMNAT). *SLAS Discov* 2020; **25**: 33–42.
39 Gjika E, Pal-Ghosh S, Tang A, *et al*. Adaptation of operational parameters of cold atmospheric plasma for *in vitro* treatment of cancer cells. *ACS Appl Mater Interfaces* 2018; **10**: 9269–9279.
40 Zhou R, Zhou R, Wang P, *et al*. Plasma-activated water: generation, origin of reactive species and biological applications. *J Phys D Appl Phys* 2020; **53**: 303001.
41 Adachi T, Nonomura S, Horiba M, *et al*. Iron stimulates plasma-activated medium-induced A549 cell injury. *Sci Rep* 2016; **6**: 20928.
42 Zhen X, Sun HN, Liu R, Choi HS, Lee DS. Non-thermal plasma-activated medium induces apoptosis of Aspc1 cells through the ROS-dependent autophagy pathway. *In Vivo* 2020; **34**: 143–153.
43 Li Y, Tang T, Lee HJ, Song K. Selective anti-cancer effects of plasma-activated medium and its high efficacy with cisplatin on hepatocellular carcinoma with cancer stem cell characteristics. *Int J Mol Sci* 2021; **22**: 3956.
44 Jo A, Bae JH, Yoon YJ, *et al*. Plasma-activated medium induces ferroptosis by depleting FSP1 in human lung cancer cells. *Cell Death Dis* 2022; **13**: 212.
45 Ying WH. $NAD^+$/NADH and $NADP^+$/NADPH in cellular functions and cell death: regulation and biological consequences. *Antioxid Redox Sign* 2008; **10**: 179–206.
46 Oehmigen K, Hähnel M, Brandenburg R, Wilke C, Weltmann KD, von Woedtke T. The role of acidification for antimicrobial activity of



doi: 10.3164/jcbn.23-112

atmospheric pressure plasma in liquids. *Plasma Process Polym* 2010; **7**: 250–257.
47 Chowdhry S, Zanca C, Rajkumar U, *et al*. NAD metabolic dependency in cancer is shaped by gene amplification and enhancer remodelling. *Nature* 2019; **569**: 570–575.